

Surface stabilized cubic phase of $CsPbI_3$ and $CsPbBr_3$ atroom temperature

Feng Yang(杨凤), Cong Wang(王聪), Yuhao Pan(潘宇浩), Xieyu Zhou(周谐宇), Xianghua Kong(孔祥华), Wei Ji(季威)

Citation: Chin. Phys. B . 2019, 28(5): 056402. **doi:** 10.1088/1674-1056/28/5/056402
Journal homepage: http://cpb.iphy.ac.cn; http://iopscience.iop.org/cpb

What follows is a list of articles you may be interested in

Anomalous behavior and phase transformation of α -GaOOH nanocrystals under static compression

Zhao Zhang(张钊), Hang Cui(崔航), Da-Peng Yang(杨大鹏), Jian Zhang(张剑), Shun-Xi Tang(汤顺熙), Si Wu(吴思), Qi-Liang Cui(崔啟良)

Chin. Phys. B . 2017, 26(10): 106402. **doi:** 10.1088/1674-1056/26/10/106402

Bending-induced phase transition in monolayer black phosphorus

Pan Dou-Xing, Wang Tzu-Chiang, Guo Wan-Lin

Chin. Phys. B . 2015, 24(8): 086401. **doi:** 10.1088/1674-1056/24/8/086401

Radial collapse and physical mechanism of carbon nanotube with divacancy and 5-8-5 defects

Zhang Ya-Ping, Ling Cui-Cui, Li Gui-Xia, Zhu Hai-Feng, Zhang Meng-Yu

Chin. Phys. B . 2015, 24(4): 046401. **doi:** 10.1088/1674-1056/24/4/046401

The nonlinear optical properties of a magneto-exciton in a strained $Ga_{0.2}In_{0.8}As$/GaAs quantum dot

N. R. Senthil Kumar, A. John Peter, Chang Kyoo Yoo

Chin. Phys. B . 2013, 22(10): 107106. **doi:** 10.1088/1674-1056/22/10/107106

Symmetry and size effects on energy and entanglement of an exciton in coupled quantum dots

Shen Man, Bai Yan-Kui, An Xing-Tao, Liu Jian-Jun

Chin. Phys. B . 2013, 22(4): 047101. **doi:** 10.1088/1674-1056/22/4/047101

Surface stabilized cubic phase of $CsPbI_3$ and $CsPbBr_3$ at room temperature*

Feng Yang(杨凤)†, Cong Wang(王聪)†, Yuhao Pan(潘宇浩), Xieyu Zhou(周谐宇), Xianghua Kong(孔祥华), and Wei Ji(季威)‡

Beijing Key Laboratory of Optoelectronic Functional Materials & Micro-Nano Devices, Department of Physics, Renmin University of China, Beijing 100872, *China*

(Received 11 March 2019; revised manuscript received 21 March 2019; published online 4 April 2019)

Inorganic halide perovskites $CsPbX_3$ (X = I, Br) have attracted tremendous attention in solar cell applications. However, the bulk form of the cubic phase $CsPbX_3$, which offers moderate direct bandgaps, is metastable at room temperature and tends to transform into a tetragonal or orthorhombic phase. Here, our density functional theory calculation results found that the surface energies of the cubic phase are smaller than those of the orthorhombic phase, although the bulk counterpart of the cubic phase is less stable than that of the orthorhombic phase. These results suggest a surface stabilization strategy to maintain the stability of the cubic phase at room temperature that an enlarged portion of surfaces shall change the relative stability of the two phases in nanostructured $CsPbX_3$. This strategy, which may potentially solve the long-standing stability issue of cubic $CsPbX_3$, was demonstrated to be feasible by our calculations in zero-, one-, and two-dimensional nanostructures. In particular, confined sizes from few to tens of nanometers could keep the cubic phase as the most thermally favored form at room temperature. Our predicted values in particular cases, such as the zero-dimensional form of $CsPbI_3$, are highly consistent with experimental values, suggesting that our model is reasonable and our results are reliable. These predicted critical sizes give the upper and lower limits of the confined sizes, which may guide experimentalists to synthesize these nanostructures and promote likely practical applications such as solar cells and flexible displays using $CsPbX_3$ nanostructures.

Keywords: inorganic perovskite solar cell, thermal stability, surface energy, nanowire, quantum dot, nanoplate

PACS: 64.70.Nd, 71.15.Mb, 84.60.Jt **DOI:** 10.1088/1674-1056/28/5/056402

1. Introduction

Organic–inorganic hybridized perovskite solar cells have recently attracted tremendous attention[1–11] because of its high power conversion efficiency (PCE),[12] low cost,[4,6,13] and manufacturing feasibility.[1,14,15] While its PCE reaches 23.7%[12] only 9 years after the first reported 3.8% in 2009,[16,17] its thermal stability issue under ultraviolet light illumination,[18] in moisture environment,[19] or at high temperatures[20] is still a challenge to the whole community. Organic–inorganic hybridize perovskite $CH_3NH_3PbI_3$ ($MAPbI_3$) tends to dissociate into volatile NH_3 and CH_3I gases[21] and PbI_2[20,22] solid under those mentioned conditions. Unfortunately, PbI_2 has a larger bandgap compared with $CH_3NH_3PbI_3$, which leads to largely reduced PCEs in perovskite solar cells. This instability was believed to be one of the most challenging issues in commercialization of perovskite solar cells.

Efforts from all aspects,such as newly designed cell architectures, substantially optimized morphology, or introduced protecting layers, have been exhaustively made to solve this issue,[13,24–27] among which large-size inorganic cations[28,29] appear to play an active role. It was found that mixing MA with larger cations, such as Cs^+, can improve the photo- and thermal-stabilities of the perovskite solar cells.[29] As a result, $CsPbI_xBr_{3-x}$ or $CsPbI_3$ shows better thermal and moisture stabilities with a reasonably high PCE of ∼10%[30–32] and a large open-circuit voltage of 1.23 V.[33] These pioneering attempts suggest another route to build practical solar cells that uses purely inorganic perovskites, like $CsPbX_3$ (X = I, Br). Another issue, however, arises that the cubic phase of inorganic perovskites, with moderate direct bandgaps of ∼ 1.7–2.0 eV and thus offering the highest performance of light absorption among all allotropes of $CsPbX_3$, is more stable at higher temperatures while their bulk form undergoes a transition to an orthorhombic phase (*Pnma*) at 578 K[34] for $CsPbI_3$ and 360 K[17] for $CsPbBr_3$ or to a tetragonal phase at 403 K[17] for $CsPbBr_3$. The room temperature orthorhombic phase has a much larger indirect bandgap, such as 2.6 eV for $CsPbI_3$,[34] compared with that of the cubic phase, which, consequently, reduces the PCE, such as 0.09% for $CsPbI_3$,[35] and light ab-

*Project supported by the National Natural Science Foundation of China (Grant Nos. 91433103, 11622437, and 61674171), the Fundamental Research Funds for the Central Universities of China, the Research Funds of Renmin University of China (Grant Nos. 16XNLQ01 and 19XNH065), and the Strategic Priority Research Program of Chinese Academy of Sciences (Grant No. XDB30000000). Cong Wang was supported by the Outstanding Innovative Talents Cultivation Funded Programs 2017 of Renmin University of China. Calculations were performed at the Physics Laboratory of High-Performance Computing of Renmin University of China and Shanghai Supercomputer Center.

†The authors contributed equally to this work.

‡Corresponding author. E-mail: wji@ruc.edu.cn

© 2019 Chinese Physical Society and IOP Publishing Ltd

sorption coefficient.

However, the stability of the cubic phase could be enhanced by downsizing its size to nanoscale where the surface energy dominates, as illustrated by $CsPbI_3$ nanocrystals[36,37] or quantum dots[33] which maintained the cubic phase for months under ambient conditions. Here, we thus comprehensively investigated the role of surface energy in tuning the cubic to orthorhombic phase transition using first-principles calculations. We considered the differences of surface energies of both the cubic and the orthorhombic phases. It turns out that the cubic phase has a higher total energy for its bulk but the surface energies of its solids are substantially lower than those of the orthorhombic phase. These competitive interactions thus lead to a reduced critical temperature for the cubic to orthorhombic phase transition if the surface ratio is enlarged. We have considered zero-, one-, and two-dimensional nanostructures while the bulk forms of both $CsPbI_3$ and $CsPbBr_3$ could be stabilized at room temperature if the crystal size is small enough. Given size and temperature dependent phase diagrams, we found characteristic sizes of 7.8–18.0 nm, 3.0–10.0 nm, 1.3–4.8 nm for 0D (nanocrystal), 1D (nanowire) and 2D (nano-plates) $CsPbI_3$, respectively, while the corresponding values are 14.0–71.9 nm, 9.7–48.3 nm, and 5.4–24.6 nm for $CsPbBr_3$. With the confined sizes smaller than these critical values, the cubic phase becomes the most stable phase at room temperature in $CsPbX_3$ nanostructures. These findings offer a feasible route to stabilize the cubic phase and to utilize these materials in solar cell applications.

2. Methods

2.1. Density functional theory calculation

Our density functional theory (DFT) calculations were performed using the generalized gradient approximation for the exchange–correlation potential, the projector augmented wave method,[38,39] and a plane-wave basis set as implemented in the Vienna *ab-initio* simulation package (VASP).[40,41] Van der Waals interactions were considered by a pairwise potential in the Grimme's 10 form (D3)[42,43] with the Becke–Jonson (BJ) form[43] for the damping function (DFT-D3-BJ). Kinetic energy cutoffs for the plane-wave basis sets were set at 600 eV and 400 eV for geometry relaxations and energy calculations, respectively. The shapes and volumes of each cell were fully optimized for bulk counterparts and all atoms were allowed to relax until the residual force on each atom was less than 0.01 eV/Å. A Γ centered $9\times9\times9$ k-mesh was used for sampling the Brillouin zone (BZ) for the cubic phases of both materials, while k-meshes of $5\times11\times3$ and $7\times7\times5$ were adopted to sample the BZs of the orthorhombic phases for $CsPbI_3$ and $CsPbBr_3$, respectively.

2.2. Surface energy

For $CsPbBr_3$, a tetragonal phase emerges between the cubic and orthorhombic phases when the temperature is in a range from 360 K to 403 K. For simplicity, we only considered the cubic and orthorhombic phases for $CsPbBr_3$ in this work, consistent with the two phases discussed in $CsPbI_3$. We considered nine surfaces for each $CsPbX_3$ in comparison of their surface energies, as shown in Fig. 3 and Table 2. There are four surfaces, which each contains Cs, Pb, and I atoms integer times those of a formula unit cell. They are the (001) surface of the cubic phase with CsI and PbI terminations on each of the surfaces, respectively [Cubic(001)-asym, Fig. 3(a)], the (010) surface of the orthorhombic phase [Orth(010), Fig. 3(b)], the I and Cs co-terminated (001) surface of the orthorhombic phase [Orth(001)-CsI, Fig. 3(c)], and the 3I terminated (100) surface of the orthorhombic phase [Orth(100)-3I, Fig. 3(d)].

The surface energy is derived using $E_{\rm Surf}=(E_{\rm Slab}-nE_{\rm CsPbX_3})/A$, where $E_{\rm Slab}$ and $E_{\rm CsPbX_3}$ are the total energies of the surface slab and the $CsPbX_3$ bulk unit cell, respectively, A is the area of the surface and n represents the number of formula unit cells that the slab contains. The surface energies of the rest surfaces are relevant to the chemical potentials of Cs, Pb, and I in forming them. In light of this, their surface energies are calculated using formula $E_{\rm Surf}=(E_{\rm Slab}-\Sigma n_i\mu_i)/A$, where n_i represents the number of atoms for the $i^{\rm th}$ element (Pb, I, Br, Cs) and μ_i represents the chemical potential of the $i^{\rm th}$ element. Here, the chemical potentials are not determinative and are in ranges estimated using $\mu_i=\mu_{\rm elem}+\Delta\mu_i$ in this work, where $\mu_{\rm elem}$ is the chemical potentials of their elementary substances and $\Delta\mu_i$ is thus the chemical potential difference of the element between in $CsPbX_3$ and in its elemental bulk counterpart. These differences satisfy $\Delta\mu_{\rm Pb}+3\Delta\mu_{\rm I/Br}+\Delta\mu_{\rm Cs}=\Delta\mu_{\rm Tot}$. Here, $\Delta\mu_{\rm Tot}$ is the total chemical potential variation of all these elements between in bulk $CsPbX_3$ and in their elementary substances, in other words, is the formation enthalpy. As a consequence, the surface energies may have three extremes: $\Delta\mu_{\rm Pb}=\Delta\mu_{\rm Tot}$; $3\Delta\mu_{\rm I/Br}=\Delta\mu_{\rm Tot}$; $\Delta\mu_{\rm Cs}=\Delta\mu_{\rm Tot}$. We summarized these results in Tables 2 and 3.

2.3. Transition temperature and confined size

At a certain temperature, the stability of the cubic phase in a nanostructure was compared with the orthorhombic phase in the same nanostructure with conserved number of atoms. Here, the free energy determines the relative stability, which includes three energy terms

$$F_{\rm Nano}=E_{\rm Nano}+T\cdot S=\sum_i A^i_{\rm Nano}\cdot E^i_{\rm surf}+V_{\rm bulk}\cdot E_{\rm bulk}+T\cdot S.$$

The first term which sums up surface energies of all types of surfaces in one configuration is the total surface energy of the nanostructure. Here, i represents the type of surfaces and $A_{\rm Nano}$ represents the corresponding surface area. The second

term is the bulk energy of the nanostructure, in which V_{bulk} represents the bulk volume in the nanostructure and E_{bulk} corresponds to the volumetric energy density of the bulk phase. The total and surface energies depend on the shape, size, and surface/bulk ratio of the nanostructures. In the last term, T and S represent temperature and entropy, respectively.

Two nanostructures at the phase transition point share the same free energy F_{Nano}. Thus we can obtain the transition temperature by calculating the volume normalized difference (ΔE_{Nano}) of the total surface energies and bulk energies between the two nanostructures

$$\Delta E_{\text{Nano}} = T \times \Delta S.$$

Volume normalized difference of entropies (ΔS) of the cubic and orthorhombic phases were estimated to be 2.0×10^{-3} meV/(K·Å^3) for $CsPbI_3$ and 1.3×10^{-3} meV/(K·Å^3) for $CsPbBr_3$, according to the experimental phase transition temperatures of bulk $CsPbX_3$.

3. Results and discussion

Figures 1(a)–1(d) show the atomic models of a $CsPbI_3$ crystal in the cubic and orthorhombic phases, respectively, while the associated lattice constants are summarized in Table 1. The cubic phase of $CsPbI_3$ [space group *Pm-3m* (No. 221)] has higher symmetry in a smaller unit cell with a lattice constant of 6.29 Å. The orthorhombic phase [*Pnma* (No. 62)] has a larger cell size with $a = 10.46$ Å, $b = 4.79$ Å, and $c = 17.81$ Å. These theoretical values are highly comparable with the experimental values with errors less than 0.5%.

Figure 1(e) plots the total energies of these two phases as a function of cell volume, which indicates that the orthorhombic phase, with a smaller equilibrium volume, is 0.29 eV more stable than the cubic phase at the zero temperature limit. The structure of the cubic phase of $CsPbBr_3$ is similar to that of $CsPbI_3$ (Fig. 2(a)). The calculated lattice constant is 5.92 Å, only 0.83% larger than the experimental value, while the orthorhombic phase of $CsPbBr_3$ is substantially different from that of $CsPbI_3$, as shown in Figs. 2(b)–2(d). The theoretical lattice constants of the orthorhombic phase are $a = 8.05$ Å, $b = 8.42$ Å, $c = 11.81$ Å with an error of less than 2% in comparison with the experimental values. Although both orthorhombic phases of $CsPbI_3$ and $CsPbBr_3$ share the same *Pnma* (D2H-16) space group, their atomic details do differ from each other. For $CsPbI_3$, Pb^{2+} ions are embedded in distorted iodine octahedra forming $(Pb_2I_6)^{2-}$ chains oriented along the y direction (Fig. 1(b)), while Cs cations are filled in the interstitial regions of these chains. Figure 1(d) clearly shows the cross-section of each $(Pb_2I_6)^{2-}$ chain, in which each Pb atom is octahedrally coordinated by six I atoms and these $(Pb_2I_6)^{2-}$ chains are alternately titled to left and right sides as arranged in a zig-zag pattern.

Table 1. Lattice parameters of bulk $CsPbI_3$ and $CsPbBr_3$ and relative errors comparing with the experimental values.

	$CsPbI_3$			$CsPbBr_3$		
	Expt.[34,44]/Å	DFT/Å	Error/%	Expt.[44,45]/Å	DFT/Å	Error/%
Cubic-a	6.29	6.29	0.00	5.87	5.92	0.85
Orth-a	10.46	10.47	0.10	8.21	8.05	−1.95
Orth-b	4.80	4.79	−0.21	8.26	8.42	1.94
Orth-c	17.78	17.81	0.17	11.76	11.81	0.43

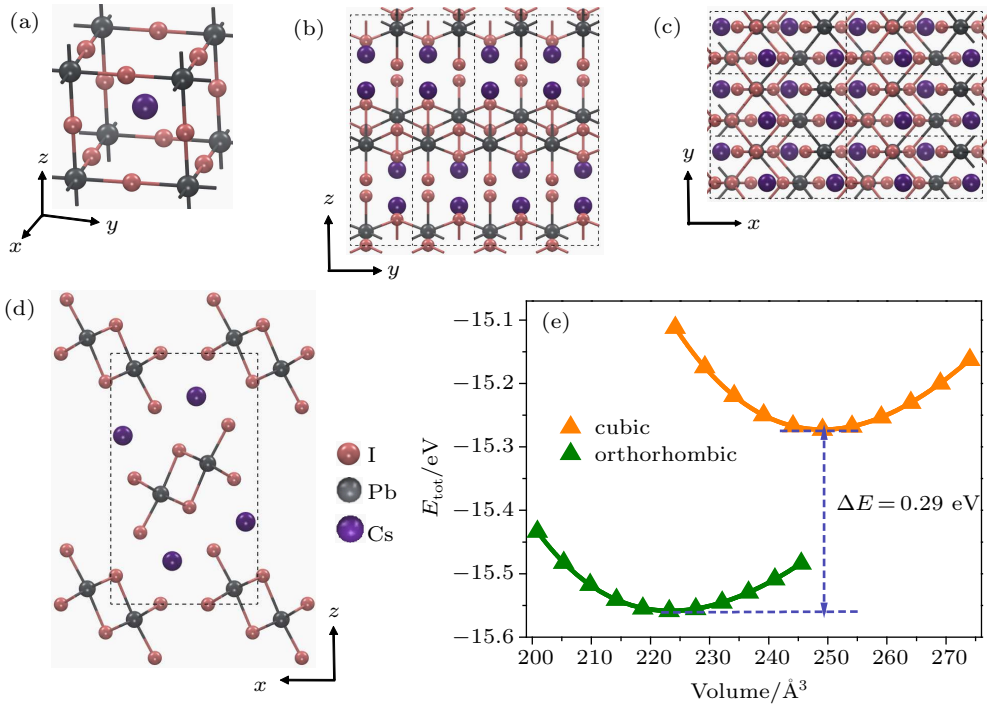


Fig. 1. Schematic models and thermal stability of bulk $CsPbI_3$ in cubic and orthorhombic phases. (a) Perspective view of the high temperature cubic phase bulk $CsPbI_3$. (b)–(d) Side- and top-views of the low temperature orthorhombic phase bulk $CsPbI_3$. Purple, gray and pink balls represent Cs, Pb and I atoms, respectively. (e) Thermal stability of bulk $CsPbI_3$ in cubic (orange line) and orthorhombic (green) phases.

In terms of $CsPbBr_3$, each Pb is again octahedrally coordinated by six I atoms, however, no chain is formed and these $(PbBr_6)^{2-}$ octahedra are continuously connected, and are slightly tilting, along all of the lattice directions forming a 3D framework, as shown in Figs. 2(c) and 2(d). Table 1 summarizes the calculated lattice constants of both phases in $CsPbI_3$ and $CsPbBr_3$, reasonably consistent with the experimental values. The energetic difference between the cubic and orthorhombic phases of $CsPbBr_3$, i.e., 0.11 eV (Fig. 2(e)), is smaller than that of $CsPbI_3$, consistent with the nearly 200 K[17,34] lowered transition temperature for $CsPbBr_3$.

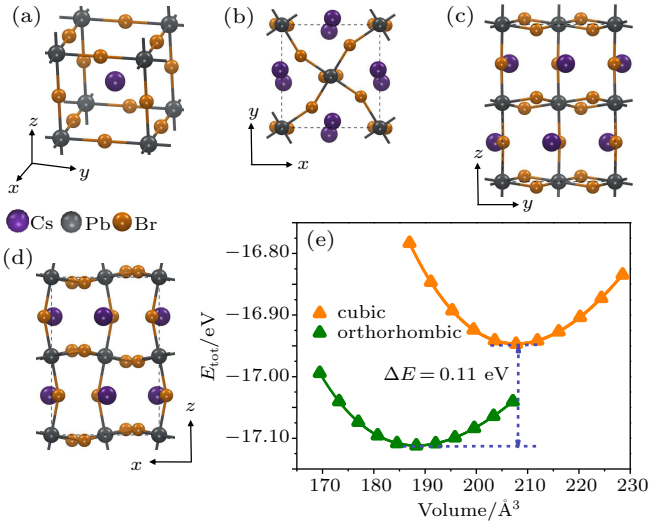


Fig. 2. Schematic models and thermal stability of bulk $CsPbBr_3$ in cubic and orthorhombic phases. (a) Perspective view of the high temperature cubic phase bulk $CsPbBr_3$. (b)–(d) Top- and side-views of the low temperature orthorhombic phase bulk $CsPbBr_3$. Purple, gray and brown balls represent Cs, Pb and Br atoms, respectively. (e) Thermal stability of bulk $CsPbBr_3$ in cubic (orange line) and orthorhombic (green) phases.

We further considered the surface energies of these phases. Energies of the surfaces Cubic(001)-asym (Fig. 3(a)), Orth(010) (Fig. 3(b)), Orth(001)-CsI (Fig. 3(c)), and Orth(100)-3I (Fig. 3(d)) are independent of the chemical potentials of the individual atoms. Among these surfaces, the first two are non-polar and the others are quasi-nonpolar. Their surface energies are 9.6 meV/Å^2, 16.0 meV/Å^2, 13.1 meV/Å^2 and 23.3 meV/Å^2, respectively (see Table 2). The first three surfaces were believed to be most stable among all surfaces considered, although the Cs rich limit of the Orth(001)-Cs (Fig. 3(e)) surface is a bit more stable than the Orth(001)-CsI surface and the I-rich limit of the Orth(100)-4I (Fig. 3(f)) surface is slightly more stable than the Orth(010) surface. Here, we emphasize that the Cs rich limit is very difficult to reach and the surface energy of the Cs-deficient limit of this surface is over 100 meV/Å^2 which is rather high compared with other surfaces (see Table 2). Although the I-rich condition is relatively more feasible to reach, its energy is comparable with that of the Orth(010) within 1 meV and the stability rapidly decreases to over 40 meV under I-deficient conditions. In light of this, we exclude both Orth(001)-Cs and Orth(100)-4I in the following discussion.

Apparently, surfaces of the cubic phase are more stable than those of the orthorhombic phase, which, again, indicates that reduced dimensions down to nanoscale could stabilize the cubic phase at room temperature. There are two terminations of surface Cubic(001), namely Cubic(001)-PbI and Cubic(001)-CsI, whose energies are in ranges from −20.4 meV/Å^2 (I rich, Cs deficient) to 59.4 meV/Å^2 (I rich, Pb deficient) and −39.8 meV/Å^2 (I rich, Pb deficient) to 39.9 meV/Å^2 (I rich, Cs deficient), respectively. Therefore, the exact surface energy of one of the surfaces is even smaller than their averaged value of 9.6 meV/Å^2, which leads to underestimated surface stability of the cubic phase. In terms of cubic $CsPbBr_3$, the $CsPbBr_3$ Cubic(001)-asym surface was used to consider the surface energy of cubic $CsPbBr_3$, which gives an surface energy of 10.9 meV/Å^2, slightly larger than that of the cubic $CsPbI_3$. The orthorhombic phase of $CsPbBr_3$ appears differently from that of cubic $CsPbI_3$, for which, we used asymmetric (001) and (110) surfaces, see Figs. 3(g) and 3(h), since the energies of these surfaces are independent of the chemical potentials of the individual atoms. Interestingly, both surfaces have the surface energy of 13.9 meV/Å^2.

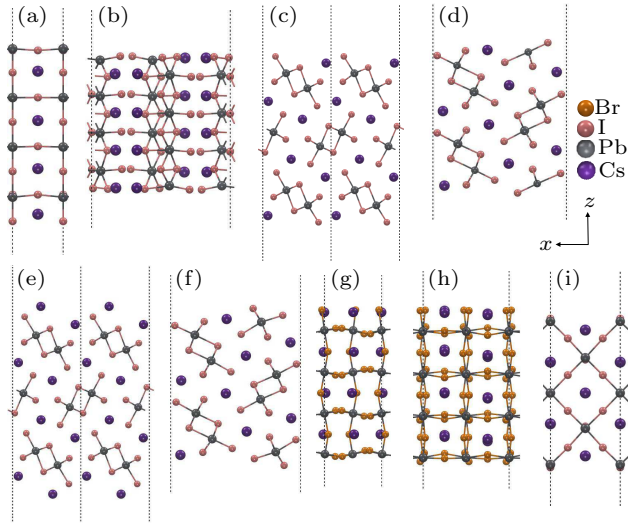


Fig. 3. Side views of surface configurations. (a) Surface (001)-asym of cubic $CsPbI_3$ with the Pb, I atoms and Cs, I atoms at the different terminations. (b) Surface (010) of orthorhombic $CsPbI_3$. (c) Surface (001)-CsI and (d) surface (100)-3I of orthorhombic $CsPbI_3$. (e) Surface (001)-Cs and (f) surface (001)-4I of orthorhombic $CsPbI_3$. (g) Surface (001)-asym and (h) surface (110)-asym of orthorhombic $CsPbBr_3$ with Pb, Br atoms and Cs, Br atoms at the different terminations. (i) Surface (110) of cubic $CsPbI_3$.

Given these surface energies, we are ready to discuss the stability of $CsPbX_3$ nanocrystals with different surface energies and surface/bulk ratios of the number atoms. In terms of one-dimensional nanostructures—i.e., nanowires—we considered five cross-section shapes for the cubic phase, as shown in Figs. 4(a)–4(d). Figures 4(a) and 4(b) show two considered triangular prisms. The one shown in Fig. 4(a) (0°-triangular prism) contains two (001) surfaces for right-angle sides and one (110) surface for the hypotenuse, which was experimentally found in a recent report,[46] while the other one is a 90°-rotated one having two (110) surfaces and one (001) surface.

Table 2. Surface energies of $CsPbI_3$.

E_{surf}/meV·Å^{-2}	Cubic				Orthorhombic				
	(001)			(110)	(100)		(010)	(001)	
	-PbI	-CsI	-asym	-	-3I	-4I	-	-CsI	-Cs
$\mu_{Pb\text{-}min}$	59.4	−39.8	9.6	53.8	23.3	15.3	16.0	13.1	7.4
$\mu_{I\text{-}min}$	32.8	−13.3	9.6	16.2	23.3	41.1	16.0	13.1	7.4
$\mu_{Cs\text{-}min}$	−20.4	39.9	9.6	26.9	23.3	15.3	16.0	13.1	138.9

Table 3. Surface energies of $CsPbBr_3$.

E_{surf}/meV·Å^{-2}	Cubic				Orthorhombic				
	(001)			(110)	(001)			(110)	
	-PbI	-CsBr	-asym	-	-PbBr	-CsBr	-asym	-PbBr	-asym
$\mu_{Pb\text{-}min}$	71.6	−49.5	10.9	73.0	78.1	−49.6	13.9	76.6	13.9
$\mu_{I\text{-}min}$	36.1	−13.9	10.9	22.7	40.7	−12.3	13.9	39.8	13.9
$\mu_{Cs\text{-}min}$	−35.1	57.3	10.9	36.5	−34.1	62.5	13.9	−33.8	13.9

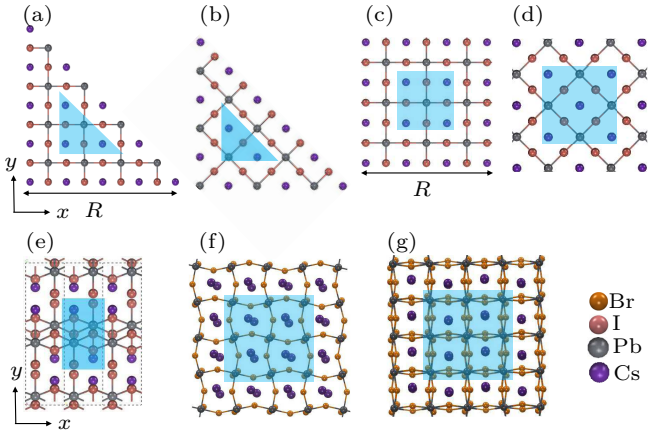


Fig. 4. Top views of 1D NWs. (a)–(e) Schematic models of $CsPbI_3$ NWs: (a) triangular prism containing two Cubic(001) surfaces for right-angle sides and one Cubic(110) surface for the hypotenuse (0°-triangular prism); (b) triangular prism having two Cubic(110) surfaces and one Cubic(001) surface (90°-triangular prism); (c) quadrangular prism with four Cubic(001) side surfaces (0°-quadrangular prism); (d) quadrangular prism with four Cubic(110) side surfaces (0°-quadrangular prism); (e) rectangular prism with Orth(010) and Orth(001)-CsI as the side surfaces. The ratio of longer and shorter edges of the rectangular cross-section is 1.22 using a criterion of maximizing the cross-section area under a given circumference. (f), (g) Schematic models of $CsPbBr_3$ NWs: (f) quadrangular prism with Orth(001)-PbBr as all the side surfaces; (g) quadrangular prism with (110) and (001) as the side surfaces.

The (110) surface of the cubic phase is depicted in Fig. 3(i) and its surface energy of 16.2 meV (Pb rich, I deficient) to 53.8 meV (I rich, Pb deficient) is rather high. A straightforward strategy thus lies in avoiding the presence of this surface. There are also two quadrangular prisms under consideration. The one shown in Fig. 4(c) (0°-quadrangular prism) has four (001) surfaces while the 90°-rotated one shown in Fig. 4(d) is cleaved along (110) surfaces. Given the total energy of the cubic phase and all surface energies, we find that the 0°-quadrangular prism is the most stable shape for cubic $CsPbI_3$ NWs, which is highly consistent with the shapes found in experiment.[47] We, therefore, use the 0°-quadrangular prism in comparison of stability with the orthorhombic phase. The shape of NWs in the orthorhombic phase is more complicated than that in the cubic phase. For simplicity, according to the experimental input,[47] we only considered the rectangular ones shown in Fig. 4(e) with optimally selected surfaces to ensure the lowest surface energies. For 2D nano-plates, we used the most stable surfaces of both phases, respectively—i.e., Cubic(001)-asym and Orth(001)-CsI—for the surface area of nano-plates. Thus, the relative stability depends on the confined thickness of the nano-plates. In terms of 0D nanoparticles, we only considered cubic nanoparticles with the Cubic(001)-asym surface for the cubic phase and the Orth(010), Orth(001)-CsI and Orth(100)-3I surfaces for the orthorhombic phase. Since the case of $CsPbBr_3$ has experimental inputs, the cross-section of $CsPbBr_3$ nanowires is considered in a square pattern, as shown in Figs. 4(f) and 4(g).

As mentioned earlier, the exact surface energy of the Cubic(001) surface is over estimated. Therefore, we consider two extremes of the (001) surface of the cubic phase, namely 9.6 meV/Å^2 and 0 meV/Å^2. The exact surface energy should be in between these two extremes while the former extreme corresponds to the minimum-size limit (red curves in Fig. 5) of a nanostructure and the zero surface energy stands for the maximum-size limit (blue curves). Figure 5 shows the phase diagrams for the cubic and orthorhombic phases as functions of temperature and size. The confined size is presented by a parameter R, which stands for the lengths of the right-angle side for triangles, the side for squares and the shorter sides of rectangles, as illustrated in Figs. 4(a) and 4(c). Here, the ratio for the longer and shorter edges of the rectangular cross-section (Fig. 4(e)) is estimated to be 1.22 using a criterion of maximizing the cross-section area under a given circumference. It explicitly shows in Fig. 5 that if R is smaller than 3.0 nm (minimum limit) to 10.0 nm (maximum limit), the cubic phase of $CsPbI_3$ becomes the most stable phase rather than the orthorhombic phase at room temperature. While the energetic difference between the two phases is smaller for $CsPbBr_3$, the critical size for phase transitions is thus larger than that of $CsPbI_3$, namely, 9.7 nm to 48.3 nm. For 2D nano-plates, the critical thicknesses to stabilize the cubic phases

are 1.3 nm to 4.8 nm for $CsPbI_3$ and 5.4 nm to 24.6 nm for $CsPbBr_3$. While the critical thickness of $CsPbI_3$ is a bit too thin, that of $CsPbBr_3$ is highly feasible that could be practically adopted in potential applications. Nanoparticles are another form of nanostructures, which were mostly explored in experiments for both solar cell and light emission applications. It shows a relative high tolerance i.e., 7.8–18 nm for $CsPbI_3$, which is consistent with the quantum dot size observed with TEM (roughly 8–15 nm) and Rietveld refinement (about 9–17 nm).[33] An even larger size of 14.0–71.9 nm is found in $CsPbBr_3$. These values are accessible in experiments, indicating the feasibility of this strategy of surface engineering for stabilizing the cubic phase of $CsPbX_3$.

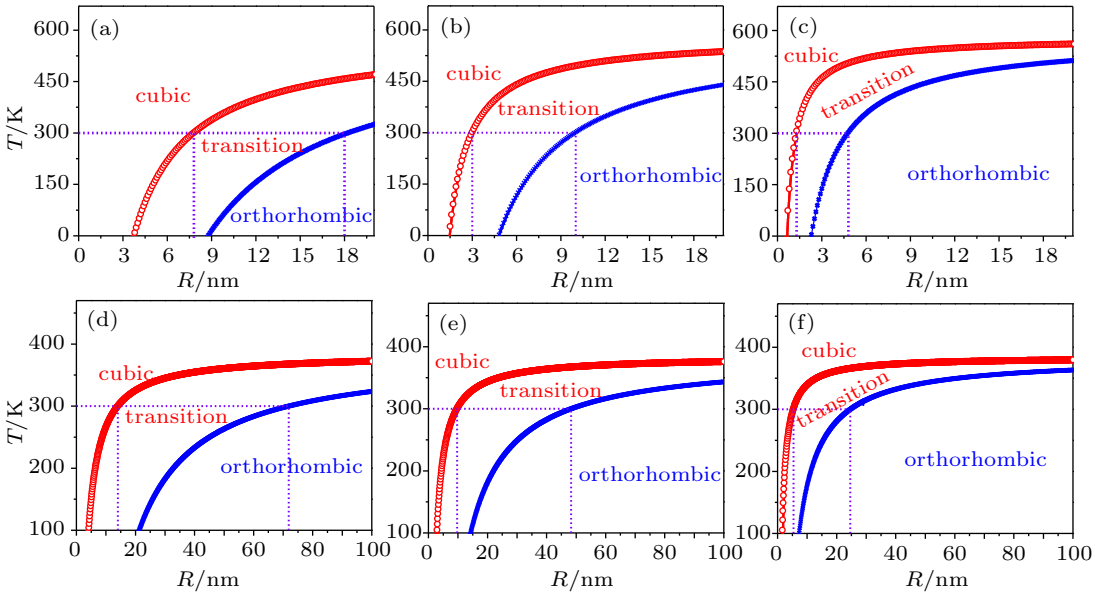


Fig. 5. Size and temperature dependent phase diagrams of $CsPbI_3$ and $CsPbBr_3$. Phase diagrams of (a) 0-dimensional, (b) 1-dimensional, and (c) 2-dimensional CsPbI3, and of (d) 0-dimensional, (e) 1-dimensional, and (f) 2-dimensional CsPbBr3. Two extremes of the (001) surface of the cubic phase were considered in the calculations. The former extreme corresponds to the minimum-size limit (surface energies of 9.6 meV/Å^2 for $CsPbI_3$ and 10.9 meV/Å^2 for $CsPbBr_3$, red curves) of a nanostructure while the maximum-size limit (blue curves) is derived by assuming a zero surface energy.

It is interesting that the critical sizes of structural phase transitions decrease with the increase of dimensions. This is straightforward to be understood that all these phase transitions are originated from energy competitions of bulk and surfaces of these two phases. The higher the dimension, the smaller the critical size. The numbers of exposed surfaces in 0D nanoparticles, 1D nanowires, and 2D nanoplates are 6, 4 and 2, respectively, leading to the decreased surface/bulk ratio with respect to the increasing dimensions. As a result, $CsPbX_3$ nanoparticles in the cubic phase shall show the excellent stability at room temperature. Indeed, there are several very recent experiments reporting potential applications of $CsPbX_3$ quantum dots or nanowires in solar cell and light emission.[48] Another noticeable phenomenon lies in the critical sizes of phase transitions for $CsPbBr_3$ usually being larger than the corresponding $CsPbI_3$ counterpart, which could be, again, explained by the smaller energy difference between the two phases of their bulk forms; i.e., 0.11 eV ($CsPbBr_3$) versus 0.29 eV ($CsPbI_3$). The larger energy difference in $CsPbI_3$ means that it needs much more surface efforts to stabilize the cubic phase of $CsPbI_3$ than that of $CsPbBr_3$. The phase diagrams here give the reference parameters for the stabilization of cubic $CsPbX_3$ in different dimensions.

4. Conclusion

In summary, this work proposes a strategy that stabilizes the meta-stable cubic phase of $CsPbX_3$ at room temperature. Density functional theory calculations were employed to illustrate the feasibility of the strategy by comparing surface and bulk energies of the cubic and orthorhombic phases with varied surface/bulk ratios. The predicted critical thickness of 2D $CsPbI_3$ nano-plates that could stabilize the cubic phase—i.e., 1.3–4.8 nm—is slightly too thin for light absorption while that of $CsPbBr_3$—i.e., 5.4–24.6 nm—may be adopted in portable or flexible display. However, the moderate sizes of the nanoparticle (7.8–71.9 nm) and nanowire (3–48.3 nm) forms appear highly promising in applications of solar cells, flexible displays, among others. In light of this, our results go one-step towards solving the long-standing stability issue of $CsPbX_3$ and may promote practical applications of nanostructured $CsPbX_3$.

References

[1] Rong Y, Hu Y, Mei A, Tan H, Saidaminov M I, Seok S I, McGehee M D, Sargent E H and Han H 2018 *Science* **361** eaat8235

[2] Liu F, Li Q and Li Z 2018 *Asian J. Org. Chem.* **7** 2182

[3] Urieta M J, Garcia B I, Molina O A and Martin N 2018 *Chem. Soc. Rev.* **47** 8541

[4] Correa B Juan P, Abate A, Saliba M, Tress W, Jesper Jacobsson T, Grätzel M and Hagfeldt A 2017 *Energy Environ. Sci.* **10** 710

[5] Huang J, Tan S, Lund P D and Zhou H 2017 *Energy Environ. Sci.* **10** 2284

[6] Li W, Wang Z, Deschler F, Gao S, Friend R H and Cheetham A K 2017 *Nat. Rev. Mater.* **2** 16099

[7] Zhou Y and Padture N P 2017 *ACS Energy Lett.* **2** 2166

[8] Wu L J, Zhao Y Q, Chen C W, Wang L Z, Liu B and Cai M Q 2016 *Chin. Phys. B* **25** 107202

[9] Li S H Li H T, Jiang Y X, Tu L M, Li W B, Pan L, Yang S E and Chen Y S 2018 *Acta Phys. Sin.* **67** 158801 (in Chinese)

[10] Zhang A Chen Y L, Yan J and Zhang C X 2018 *Acta Phys. Sin.* **67** 106701 (in Chinese)

[11] Zhang Y Y, Chen S Y, Xu P, Xiang H, Gong X G, Walsh A and Wei S H 2018 *Chin. Phys. Lett.* **35** 036104

[12] https://www.nrel.gov/pv/cell-efficiency.html

[13] Green M A, Ho-Baillie A and Snaith H J 2014 *Nat. Photonics* **8** 506

[14] Jung H S and Park N G 2015 *Small* **11** 10

[15] Ma Y, Wang S, Zheng L, Lu Z, Zhang D, Bian Z, Huang C and Xiao L 2014 *Chin J. Chem.* **32** 957

[16] Kojima A, Teshima K, Shirai Y and Miyasaka T 2009 *J. Am. Chem. Soc.* **131** 6050

[17] Stoumpos C C, Malliakas C D, Peters J A, Liu Z, Sebastian M, Im J, Chasapis T C, Wibowo A C, Chung D Y, Freeman A J, Wessels B W and Kanatzidis M G 2013 *Cryst. Growth Des.* **13** 2722

[18] Leijtens T, Eperon G E, Pathak S, Abate A, Lee M M and Snaith H J 2013 *Nat. Commun.* **4** 2885

[19] Li B, Fei C, Zheng K, Qu X, Pullerits T, Cao G and Tian J 2016 *J. Mater. Chem. A* **4** 17018

[20] Conings B, Drijkoningen J, Gauquelin N, Babayigit A, D'Haen J, D'Olieslaeger L, Ethirajan A, Verbeeck J, Manca J, Mosconi E, Angelis F D and Boyen H G 2015 *Adv. Energy. Mater.* **5** 1500477

[21] Juarez-Perez E J, Hawash Z, Raga S R, Ono L K and Qi Y 2016 *Energy Environ. Sci.* **9** 3406

[22] Nenon D P, Christians J A, Wheeler L M, Blackburn J L, Sanehira E M, Dou B, Olsen M L, Zhu K, Berry J J and Luther J M 2016 *Energy Environ. Sci.* **9** 2072

[23] Berhe T A, Su W N, Chen C H, Pan C J, Cheng J H, Chen H M, Tsai M C, Chen L Y, Dubale A A and Hwang B J 2016 *Energy Environ. Sci.* **9** 323

[24] Li X, Cao F, Yu D, Chen J, Sun Z, Shen Y, Zhu Y, Wang L, Wei Y, Wu Y and Zeng H 2017 *Small* **13** 1603996

[25] Correa-Baena J P, Abate A, Saliba M, Tress W, Jacobsson T J, Grätzel M and Hagfeldt A 2017 *Energy Environ. Sci.* **10** 710

[26] Yin W J, Yang J H, Kang J, Yan Y and Wei S H 2015 *J. Mater. Chem. A* **3** 8926

[27] Shi Z, Guo J, Chen Y, Li Q, Pan Y, Zhang H, Xia Y and Huang W 2017 *Adv. Mater.* **29** 1605005

[28] Yuan Y, Xu R, Xu H T, Hong F, Xu F and Wang L J 2015 *Chin. Phys. B* **24** 116302

[29] McMeekin D P, Sadoughi G, Rehman W, Eperon G E, Saliba M, Horantner M T, Haghighirad A, Sakai N, Korte L, Rech B, Johnston M B, Herz L M and Snaith H J 2016 *Science* **351** 151

[30] Saliba M, Matsui T, Seo J Y, Domanski K, Correa-Baena J P, NazeeruddinMK, Zakeeruddin S M, TressW, Abate A and Hagfeldt A 2016 *Energy Environ. Sci.* **9** 1989

[31] Zheng J J Wang Y R, Yu K H, Xu X X, Sheng X X, Hu E T and W W 2018 *Acta Phys. Sin.* **67** 118502 (in Chinese)

[32] Sutton R J, Eperon G E, Miranda L, Parrott E S, Kamino B A, Patel J B, Hörantner M T, Johnston M B, Haghighirad A A, Moore D T and Snaith H J 2016 *Adv. Energy. Mater.* **6** 1502458

[33] Swarnkar A, Marshall A R, Sanehira E M, Chernomordik B D, Moore D T, Christians J A, Chakrabarti T and Luther J M 2016 *Science* **354** 92

[34] Trots D M and Myagkota S V 2008 *J. Phys. Chem. Solids* **69** 2520

[35] Choi H, Jeong J, Kim H B, Kim S, Walker B, Kim G H and Kim J Y 2014 *Nano Energy* **7** 80

[36] Eperon G E, Patern'o G M, Sutton R J, Zampetti A, Haghighirad A A, Cacialli F and Snaith H J 2015 *J. Mater. Chem. A* **3** 19688

[37] Protesescu L, Yakunin S, Bodnarchuk M I, Krieg F, Caputo R, Hendon C H, Yang R X, Walsh A and Kovalenko M V 2015 *Nano Lett.* **15** 3692

[38] Blöchl P E 1994 *Phys. Rev. B* **50** 17953

[39] Kresse G and Joubert D 1999 *Phys. Rev. B* **59** 1758

[40] Kresse G and Furthmüller J 1996 *Comp. Mater. Sci.* **6** 15

[41] Kresse G and Furthmüller J 1996 *Phys. Rev. B* **54** 11169

[42] Grimme S, Antony J, Ehrlich S and Krieg H 2010 *J. Chem. Phys.* **132** 154104

[43] Grimme S, Ehrlich S and Goerigk L 2011 *J. Comp. Chem.* **32** 1456

[44] Jiang L Q, Guo J K, Liu H B, Zhu M, Zhou X, Wu P and Li C H 2006 *J. Phys. Chem. Solids* **67** 1531

[45] Rodová M, Brožek J, Knížek K. and Nitsch K 2003 *J. Therm. Anal. Calorim.* **71** 667

[46] Wang Y, Sun X, Shivanna R, Yang Y, Chen Z, Guo Y, Wang G C, Wertz E, Deschler F and Cai Z 2016 *Nano. Lett.* **16** 7974

[47] Zhang D, Eaton S W, Yu Y, Dou L and Yang P 2015 *J. Am. Chem. Soc.* **137** 9230

[48] Liao J F, Li W G, Rao H S, Chen B X, Wang X D, Chen H Y and Kuang D B 2017 *Sci. China Mater.* **60** 285